

THE LOGARITHMIC SPIRAL AND ITS SPHERICAL COUNTERPART

Abstract: Logarithmic spirals are isogonal trajectories of pencils of lines. From a series of geometric consequences, we pick out a few which are relevant for kinematics: When a logarithmic spiral rolls on a line, its asymptotic point traces a straight line. Hence, wheels with the shape of a logarithmic spiral can be used for a stair climbing robot. When involute spur gears are to be generated by virtue of the principle of Camus, the auxiliary pitch curves must be logarithmic spirals. Two congruent logarithmic spirals can roll on each other while their asymptotic points remain fixed. A composition of two such rollings gives a two-parametric motion which allows a second decomposition of this kind. Some of these properties hold similarly for the spherical counterparts, the spherical loxodromes. For example, when in spherical geometry a loxodrome rolls on a circle, both asymptotic points trace circular involutes. Therefore, spherical loxodromes are auxiliary pitch curves for involute bevel gearing. On the other hand, spherical loxodromes can also be seen as helical curves in the projective model of hyperbolic geometry, where the sphere serves as a Clifford surface. This paves the way for remarkable arrangements of loxodromes on a sphere, e.g., a 3-web.

Key words: logarithmic spiral, involute spur gears, two-parametric motion, spherical loxodrome, involute bevel gears, hyperbolic screws, 3-web.

INTRODUCTION

The logarithmic spiral, displayed in Fig. 1, was first disclosed by René Descartes (1596–1650), who called this curve *equiangular spiral*. Evangelista Torricelli (1608–1647) rectified this curve in 1645, even before calculus was invented by Newton and Leibnitz. The sobriquet, *logarithmic*, was given to this spiral by Jakob Bernoulli (1654–1705). Bernoulli was so fascinated by this curve that he investigated its properties in depth and went up to demanding that such a spiral be engraved on his tombstone with the phrase “*Eadem mutata resurgo*”, which means “Although changed, I shall arise the same”, in agreement with its self-similarity property. Unfortunately, the sculptor of Bernoulli’s tombstone made the mistake of sculpting, instead, an Archimedean spiral (see Fig. 2b).

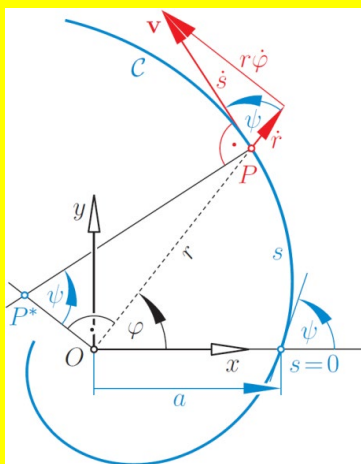


Fig. 1 Logarithmic spiral C and its velocity vector v at point P .

First examples on the synthesis of involute cylindrical gears via the logarithmic spiral as auxiliary centrode,

when applying the Camus theorem, can be found in Reuleaux’s book [18], along with the books of Airy [1], Bennett [2], and Willis [20], which are also cited by Reuleaux.



(a) (b)

Fig. 2 Jakob Bernoulli: (a) Memorial plaque in the Minster in Basel/Switzerland; (b) Zoom-in of the legend “*Eadem mutata resurgo*” along with the wrong spiral.

The spherical logarithmic spiral, also known as the loxodromic spiral, is the analogue of the planar logarithmic spiral in spherical geometry. It gained particular interest in navigation since it gives a constant-bearing course on the Earth, as it intersects all the meridians at the same angle. Pictures of spherical loxodromes can also be found in the work of Escher, such as the “*Sphere Spirals*” and “*Sphere Surface with Fish*” [3], p. 319, as shown in Fig. 3.

Similar to involute cylindrical gears, the synthesis of exact involute bevel gears is formulated in this paper by application of the Camus Theorem and assuming a spherical logarithmic spiral as auxiliary centrode, which rolls on the pitch circles of the fundamental sphere. Con-

sequently, the pole traces the exact spherical involute directly, without using the base circles or applying envelope theory, which would yield octoidal gears rather than involute gears (cf [9]).



Fig. 3 M. C. Escher’s 1958 woodcuts “Sphere Spirals” and “Sphere Surface with Fish” [3].

Concerning gears with skew axes, the Ball-Disteli diagram is extremely useful to synthesize spatial gears via the Camus theorem. In this context, the orthogonal helicoid plays the role of the auxiliary surface to generate the tooth flanks of involute-gear pairs with skew axes, even if they show interpenetration, as described in previous publications [11, 12]. As an alternative, the synthesis of the pitch surfaces of non-circular skew-gears was proposed in [10], whereby the case of identical logarithmic spirals was also developed. This could be also useful to synthesize the spatial version of the logarithmic spiral and the skew involute gears.

2. ROLLING LOGARITHMIC SPIRALS

Usually, a logarithmic spiral \mathcal{C} is defined by its polar equation

$$\mathcal{C}: r(\varphi) = ae^{b\varphi}, \tag{2.1}$$

depending on the two real constants $a = r(0) > 0$ and $b \in \mathbb{R} \setminus \{0\}$. The origin O is the asymptotic point, obtained as the limit for $(b\varphi) \rightarrow -\infty$.

Let the polar angle be given by the smooth monotonic function $\varphi(t)$. This gives rise to the parametrization in cartesian coordinates, namely

$$\mathbf{c}(t) = r(\varphi(t)) \begin{pmatrix} \cos \varphi(t) \\ \sin \varphi(t) \end{pmatrix}. \tag{2.2}$$

Differentiation by t yields the velocity vector

$$\mathbf{v}(t) = \dot{\mathbf{c}}(t) = \dot{r} \begin{pmatrix} \cos \varphi \\ \sin \varphi \end{pmatrix} + r\dot{\varphi} \begin{pmatrix} -\sin \varphi \\ \cos \varphi \end{pmatrix},$$

decomposed into two orthogonal components (Fig. 1). If $s(t) = \|\dot{\mathbf{c}}(t)\|$ denotes the arc length of \mathcal{C} , we obtain for the angle ψ between the radial direction and the velocity vector \mathbf{v} , from eq. (2.1),

$$\cot \psi = \frac{\dot{r}}{r\dot{\varphi}} = \frac{br\dot{\varphi}}{r\dot{\varphi}} = b = \text{const.} \tag{2.3}$$

Moreover, we conclude from

$$\frac{dr}{ds} = \frac{\dot{r}}{\dot{s}} = \cos \psi$$

that ψ is constant if and only if the polar radius r is a linear function of the arc length s .

Lemma 1: *Logarithmic spirals are characterized by the polar distance r being a linear function of arc length s .*

By virtue of the foregoing Lemma, it is apparent that the spiral and related motions under study can be analyzed upon using r or s as parameter, playing the same role as time t . Hence, differentiation with respect to (w.r.t., in brief) s produces time rates of change in our analysis.

We specify $\mathbf{c}(0)$ as the initial point for the arc length and assume that, for $b > 0$, the arc length s grows monotonically with r . Then we obtain the arc length parametrization of the logarithmic spiral by plugging

$$r(s) = a + s \cos \psi, \quad \varphi(s) = \frac{1}{b} \ln \left(1 + \frac{\cos \psi}{a} s \right) \tag{2.4}$$

into eq. (2.2). Due to the condition $r > 0$, the parameter s must be restricted to

$$s > \frac{-a}{\cos \psi},$$

thereby revealing that the arc length from the initial point to the asymptotic point equals $(a/\cos \psi)$. Well-known formulas yield, for the curvature $\kappa(s)$ and the radius of curvature $\rho(s)$

$$\kappa = \frac{d\kappa}{ds} = \frac{d\varphi}{dr} \frac{dr}{ds} = \frac{1}{br} \cos \psi = \frac{\sin \psi}{r}, \quad \rho = \frac{r}{\sin \psi}.$$

This explains the construction of the center of curvature P^* corresponding to point $P \in \mathcal{C}$, as shown in Fig. 1.

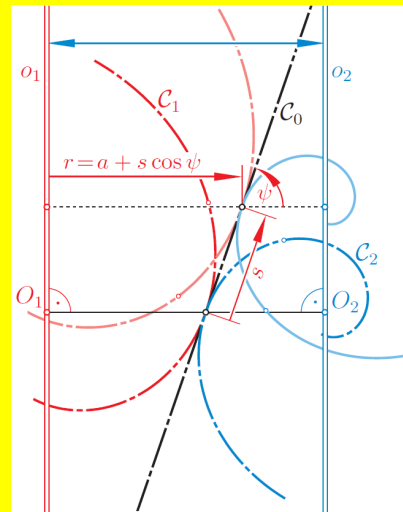


Fig. 4 Two logarithmic spirals \mathcal{C}_1 and \mathcal{C}_2 roll simultaneously on a line \mathcal{C}_0 .

When a logarithmic spiral \mathcal{C}_1 rolls on a line \mathcal{C}_0 , the asymptotic point O_1 of \mathcal{C}_1 traces a line o_1 (Fig. 4), which follows from Lemma 1, but can also be derived from kinematics: The spiral \mathcal{C}_1 and the fixed line \mathcal{C}_0 are the pitch curves of the motion of interest, while the instantaneous tangent of O_1 is orthogonal to the connection with the pitch point, i.e., the point of contact between \mathcal{C}_1 and \mathcal{C}_0 .



Fig. 5 Staircase climber (photo: Online catalogue of kinematic models, Institute of Discrete Mathematics and Geometry, TU Vienna, <http://www.geometrie.tuwien.ac.at/kinmodelle/>).

As an application, Fig. 5 shows how the logarithmic spiral can be used for a stairclimbing device (cf [15], [17]).

Let us return to Fig. 4: When another logarithmic spiral \mathcal{C}_2 rolls simultaneously on \mathcal{C}_0 its asymptotic point O_2 traces a line o_2 parallel to o_1 . Hence, the distance between O_1 and O_2 remains constant. Thus, the inverse motion keeps both points O_1 and O_2 fixed, while the directly congruent logarithmic spirals \mathcal{C}_1 and \mathcal{C}_2 roll on each other (Fig. 6). Examples of this rolling can be found in the literature [8], pp. 128–129, and in [21], p. 232.

The transmission between the rotations about O_1 and O_2 via the two spirals can also be explained with Lemma 1 and the first of eqs. (2.4). During the depicted external rolling by length s , the distance between O_1 and the point of contact between \mathcal{C}_1 and \mathcal{C}_2 , the pitch point, increases by $(s \cos \psi)$, while the distance between O_2 and the pitch point decreases about the same amount. However, this motion with pitch curves \mathcal{C}_1 and \mathcal{C}_2 is also possible in the case of internal rolling, when the pitch point lies outside the segment O_1O_2 and both distances increase by the same amount.

It makes sense to define the constant a in the polar equation (2.1) of a logarithmic spiral as the x -coordinate of the initial point ($s = 0$) of the spiral (note Fig. 1). Then, in the case of internal rolling, the respective constants a_1, a_2 of the two pitch curves have equal signs. Otherwise their signs differ.

Let us turn over to the usual kinematic setting: We assume that the two spirals \mathcal{C}_1 and \mathcal{C}_2 are correspondingly attached two the systems (i.e., frames) Σ_1 and Σ_2 , which move w.r.t. the fixed frame Σ_0 .

By virtue of a basic theorem from kinematics, the signed distances of the centers O_1 and O_2 to the pitch point define the instant transmission ratio, i.e., the ratio between the angular velocities ω_{10} and ω_{20} of the two moving frames Σ_1 and Σ_2 w.r.t. Σ_0 . As per our conven-

tion concerning the signs of the constants a_1 and a_2 , we can state for the transmission ratio, in terms of the arc length s of the pitch curves,

$$\omega_{10} : \omega_{20} = (a_2 + s \cos \psi) : (a_1 + s \cos \psi). \quad (2.5)$$

This works for internal as well as for external rolling, provided that the constant $b = \cot \psi$ is the same for both spirals.

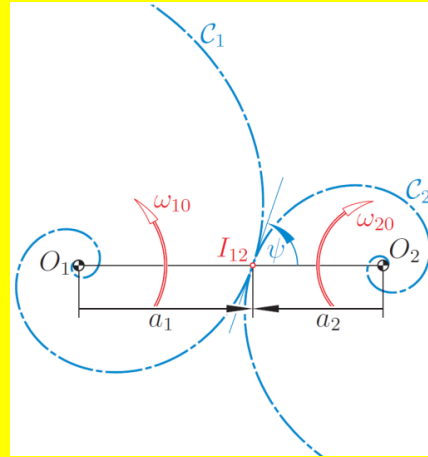


Fig. 6 Non-uniform transmission via rolling logarithmic spirals.

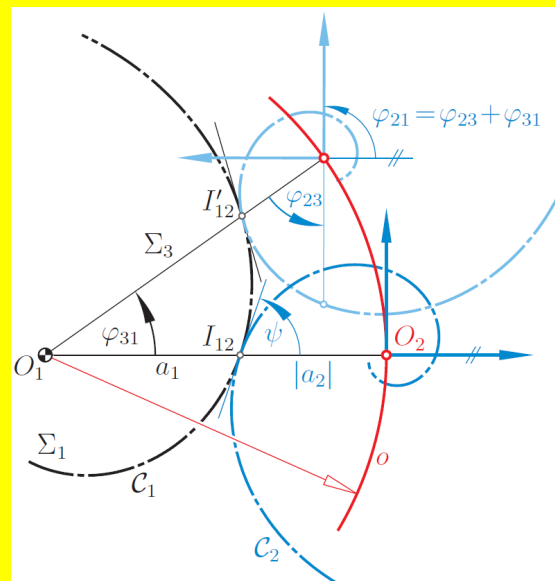


Fig. 7 When the logarithmic spiral \mathcal{C}_2 rolls on the congruent fixed spiral \mathcal{C}_1 , the asymptotic point O_2 traces a circle o .

The same can be confirmed by studying the angles of rotation $\varphi_{10}, \varphi_{20}$ of Σ_1 and Σ_2 , respectively, from the initial pose $s = 0$ on: From the second of eqs. (2.4), we obtain

$$\varphi_{10}(s) = \frac{1}{b} \ln \left(1 + \frac{\cos \psi}{a_1} \right), \quad \varphi_{20}(s) = \frac{1}{b} \ln \left(1 + \frac{\cos \psi}{a_2} \right) \quad (2.6)$$

Differentiation of the foregoing expression w.r.t. s yields

$$\begin{aligned} \dot{\varphi}_{10} : \dot{\varphi}_{20} &= \frac{a_1 \cos \psi}{(a_1 + s \cos \psi)a_1} : \frac{a_2 \cos \psi}{(a_2 + s \cos \psi)a_2} \\ &= (a_2 + s \cos \psi) : (a_1 + s \cos \psi) = \omega_{10} : \omega_{20}. \end{aligned}$$

Now we study the relative motion Σ_2/Σ_1 , with the spiral \mathcal{C}_2 rolling along the fixed centrod \mathcal{C}_1 (Fig. 7). In

The Logarithmic Spiral and its Spherical Counterpart

this case the asymptotic point O_2 traces a circle o centered at O_1 .

Let Σ_3 denote the frame attached to the bar O_1O_2 . Then, by virtue of (2.6), the angles of rotation of Σ_1 and Σ_2 w.r.t. Σ_3 are

$$\varphi_{13}(s) = \frac{1}{b} \ln \left(1 + \frac{\cos \psi}{a_1} \right), \quad \varphi_{23}(s) = \frac{1}{b} \ln \left(1 + \frac{\cos \psi}{a_2} \right),$$

where $\varphi_{21} = \varphi_{23} + \varphi_{31} = \varphi_{23} - \varphi_{13}$. Therefore,

$$\varphi_{21} = \frac{1}{b} \ln \left(\frac{1 + \sigma/a_2}{1 + \sigma/a_1} \right), \quad \text{where } \sigma := s \cos \psi. \quad (2.7)$$

In 1913, R. Bricard studied the composition of two independent rollings Σ_2/Σ_1 and Σ_3/Σ_2 of pairs of logarithmic spirals $(\mathcal{C}_2, \mathcal{C}_1)$ and $(\mathcal{C}_3, \mathcal{C}_2')$, where all spirals are directly congruent and the two spirals \mathcal{C}_2 and \mathcal{C}_2' , both attached to Σ_2 , share the asymptotic point O_2 .

Bricard stated the result below, without a proof.

Theorem 1. (R. Bricard [4], p. 23, sect. 3) *The composition of two rollings Σ_2/Σ_1 and Σ_3/Σ_2 of directly congruent logarithmic spirals $(\mathcal{C}_1, \mathcal{C}_2)$ and $(\mathcal{C}_2', \mathcal{C}_3)$, where $\mathcal{C}_2, \mathcal{C}_2' \subset \Sigma_2$ share the asymptotic point O_2 , has a second decomposition of the same type with spirals $(\tilde{\mathcal{C}}_1, \tilde{\mathcal{C}}_2)$ and $(\tilde{\mathcal{C}}_2', \tilde{\mathcal{C}}_3)$. The respective asymptotic points $O_1, O_2, O_3, \tilde{O}_2$ form a parallelogram (Fig. 8).*

Remark 1. This is one of the rather rare examples of twofold-decomposable motions. Up to recently, less than 20 cases were known in the Euclidean 2- or 3-space (note [19], Table I). When W. Blaschke posed the question in 1938, about such two-parametric motions, he was not aware that 25 years earlier G. Koenigs [14] had already posed the same question, while providing, besides R. Bricard [4, 5, 6, 7], the first examples.

Proof: We denote with Σ_4 and Σ_5 the frames attached to the bars O_1O_2 and O_2O_3 (note Fig. 8), respectively. Furthermore, the first motion parameter s is the arc length of the first pair of rolling spirals $(\mathcal{C}_1, \mathcal{C}_2)$, and the second parameter t being the arc length of the second pair $(\mathcal{C}_2', \mathcal{C}_3)$. The pairs of reals (a_1, a_2) and (a_2', a_3) are the signed initial radii of the two spirals at play, in accordance with the convention explained above.

Then, by virtue of eqs. (2.6) and (2.7), we obtain, for the respective angles of rotation,

$$\begin{aligned} \varphi_{41} &= \frac{1}{b} \ln(1 + \sigma/a_1), \quad \sigma = s \cos \psi, \\ \varphi_{51} &= \frac{1}{b} \ln \left(\frac{1 + \sigma/a_1}{1 + \sigma/a_2} (1 + \tau/a_2') \right), \quad \tau = t \cos \psi, \\ \varphi_{31} &= \frac{1}{b} \ln \left(\frac{1 + \sigma/a_1}{1 + \sigma/a_2} \frac{1 + \tau/a_2'}{1 + \tau/a_3} \right). \end{aligned}$$

Now we extend the triangle $O_1O_2O_3$ of asymptotic points by \tilde{O}_2 to a parallelogram and seek two other pairs of logarithmic spirals $(\tilde{\mathcal{C}}_1, \tilde{\mathcal{C}}_2)$ and $(\tilde{\mathcal{C}}_2', \tilde{\mathcal{C}}_3)$ that produce the same composition. Further frames are introduced, namely, $\tilde{\Sigma}_2, \tilde{\Sigma}_4$ and $\tilde{\Sigma}_5$. The new motion para-

eters are \tilde{s} and \tilde{t} , besides the definitions $\tilde{\sigma} = \tilde{s} \cos \psi$ and $\tilde{\tau} = \tilde{t} \cos \psi$. The new constants of the spirals are $\tilde{a}_1, \tilde{a}_2, \tilde{a}_2'$ and \tilde{a}_3 . Parallelity between opposite sides leads to the new angles of rotations, namely,

$$\tilde{\varphi}_{51} = \varphi_{41}, \quad \tilde{\varphi}_{41} = \varphi_{51} \quad \text{and} \quad \tilde{\varphi}_{31} = \varphi_{31},$$

where the related side lengths satisfy $a_2 - a_1 = \tilde{a}_3 - \tilde{a}_2'$ and $a_3 - a_2' = \tilde{a}_2 - \tilde{a}_1$.

After some computations it turns out that the foregoing conditions can be satisfied by setting

$$\begin{aligned} \tilde{a}_1 &= \frac{a_1 a_2'}{a_2}, \quad \tilde{a}_2 = \frac{a_1 a_2' + a_2 a_3 - a_2 a_2'}{a_2}, \\ \tilde{a}_2' &= \frac{a_1 a_2' + a_2 a_3 - a_2 a_2'}{a_2'}, \quad \tilde{a}_3 = \frac{a_2 a_3}{a_2'} \end{aligned}$$

and

$$\tilde{\sigma} = \frac{(a_1 + \sigma)(a_2' + \tau)}{(a_2 + \sigma)} - \frac{a_1 a_2'}{a_2}, \quad \tilde{\tau} = \frac{(a_2 + \sigma)(a_3 + \tau)}{(a_2' + \sigma)} - \frac{a_2 a_3}{a_2'}.$$

The two decompositions satisfy the symmetric relations

$$a_2 \tilde{a}_2 = a_2' \tilde{a}_2' \quad \text{and} \quad (a_2 + \sigma)(\tilde{a}_2 + \tilde{\sigma}) = (a_2' + \tau)(\tilde{a}_2' + \tilde{\tau}).$$

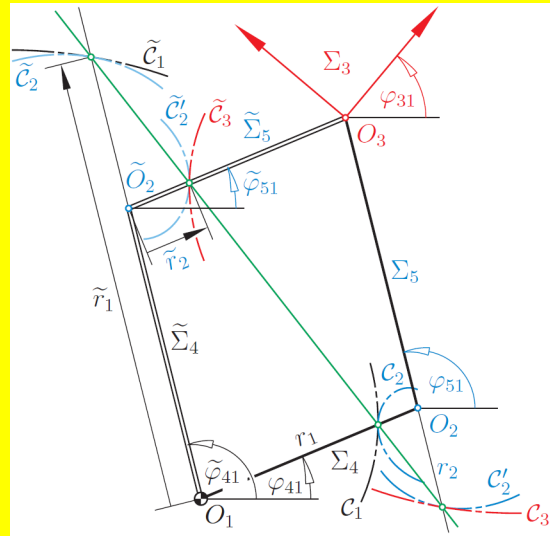


Fig. 8 A two-parametric motion Σ_3/Σ_1 which is twofold-decomposable.

A well-known theorem from the kinematics of two-parameter motions implies that at each instant the pitch points of the four rollings at play have to be aligned. This is illustrated in Fig. 8. The distances of the respective pitch points to O_1, O_2 and \tilde{O}_2 are denoted by (r_1, r_2) and $(\tilde{r}_1, \tilde{r}_2)$, where $r_1 = a_1 + \sigma, r_2 = a_2' + \tau, \tilde{r}_1 = \tilde{a}_1 + \tilde{\sigma}$ and $\tilde{r}_2 = \tilde{a}_2' + \tilde{\tau}$. □

There is another interesting case where a logarithmic spiral \mathcal{C}_2 rolls on a fixed spiral \mathcal{C}_1 (Fig. 9). This time the spirals need not be congruent, but at each instant the arc-lengths between the point of contact and the respective asymptotic points must be equal. Therefore, each point of the two spirals becomes a pitch point during the motion. In this case we speak of a *global* rolling of \mathcal{C}_2 on \mathcal{C}_1 . This implies, for the shape parameters (a_1, ψ_1) of \mathcal{C}_1 and (a_2, ψ_2) of \mathcal{C}_2 , the condition

$$\frac{a_1}{\cos \psi_1} = \frac{a_2}{\cos \psi_2}.$$

This means that, geometrically speaking, in the initial pose $s = 0$ the circumcircle of O_1 , O_2 and the pitch point I_{12} is centered on the common tangent at I_{12} (note Fig. 9). Hence, by virtue of the first of eqs. (2.4), the ratio between corresponding polar radii r_1 and r_2 satisfies

$$r_1 : r_2 = \left(\frac{a_1}{\cos \psi_1} + s \right) \cos \psi_1 : \left(\frac{a_2}{\cos \psi_2} + s \right) \cos \psi_2 = \text{const.}$$

Therefore, in all poses of \mathcal{C}_2 , the triangles formed by the asymptotic points O_1 , O_2 of the spirals and the pitch point I_{12} are mutually similar. This is valid for external as well as for internal global rollings.

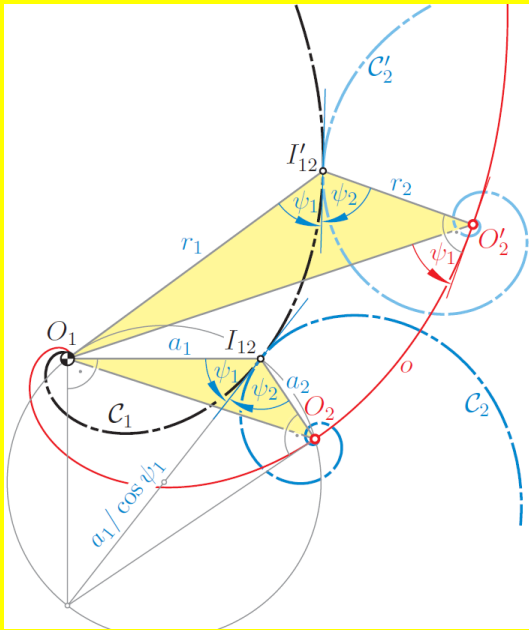


Fig. 9 During a ‘global’ rolling of \mathcal{C}_2 on \mathcal{C}_1 the asymptotic point O_2 traces a spiral o congruent to \mathcal{C}_1 .

When a logarithmic spiral \mathcal{C}_2 rolls on a circle \mathcal{C}_1 with radius R then the asymptotic point O_2 of \mathcal{C}_2 traces an involute o to the circle b_1 with radius $(R \cos \psi)$. We reach this conclusion from the observation that each path-normal connects O_2 with the instant pitch point I_{12} , and thereby intersecting the circle \mathcal{C}_1 under the constant angle ψ . Hence, all path-normals envelope a circle b_1 concentric with \mathcal{C}_1 (note Fig. 10).

Consequently, the logarithmic spiral serves as auxiliary curve when the tooth profiles of involute gears are generated by Camus' principle (see, e.g., [21], p. 212). The profiles \mathcal{C}_2 , \mathcal{C}_3 , involutes of the base circles b_2 , b_3 , are the trajectories of the asymptotic point O when a logarithmic spiral p_4 rolls on the pitch circles p_2 and p_3 , respectively (Fig. 11).

In total, two logarithmic spirals, one on each side of the pitch circles, are necessary for the complete tooth profiles.

The foregoing results are summarized below:

Theorem 2: Table 1 shows the trajectories of the asymptotic point O_2 of a logarithmic spiral \mathcal{C}_2 rolling on specific curves.

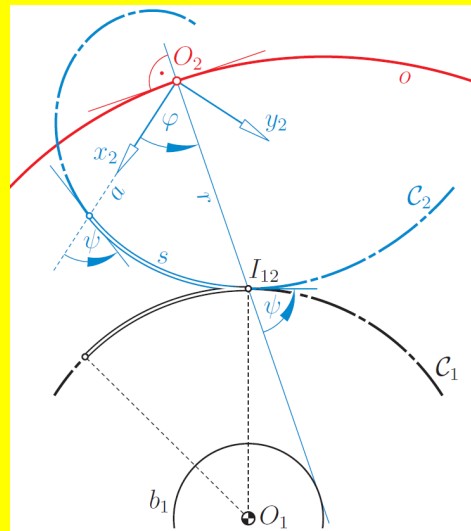


Fig. 10 When the logarithmic spiral \mathcal{C}_2 rolls on the circle \mathcal{C}_1 , the asymptotic point O_2 of \mathcal{C}_2 traces an involute o of the base circle b_1 .

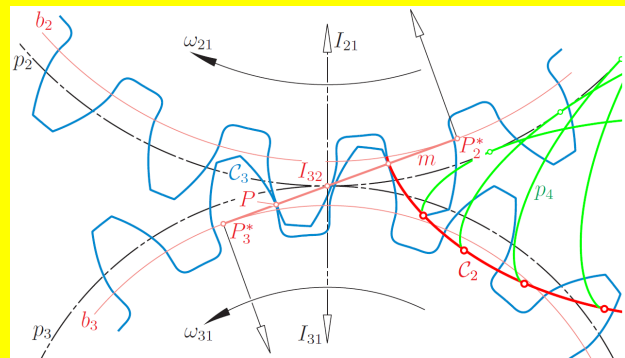


Fig. 11 Involute gears with meshing line m , generated according to the Camus principle with the auxiliary pitch curve p_4 , a logarithmic spiral with $\psi = 20^\circ$.

Table 1

Rolling logarithmic spirals

logarithmic spiral \mathcal{C}_2 rolls	path of asymptotic point O_2	Figs.
on a straight line \mathcal{C}_0	straight line	Fig. 4
on a congruent logarithmic spiral \mathcal{C}_1	circle centered at the pole O_1 of \mathcal{C}_1	Fig. 7
globally on an incongruent log. spiral \mathcal{C}_1	spiral congruent to \mathcal{C}_1	Fig. 9
on a circle \mathcal{C}_1	involute of a concentric circle b_1	Fig. 10

3. ROLLING SPHERICAL LOXODROMES

In order to obtain the spherical analogue of logarithmic spirals, we assume that a logarithmic spiral lies in the xy -plane in three-dimensional space, and apply the stereographic projection onto the unit sphere with projection center at the South pole $S = (0,0,-1)$ (see Fig. 12). While the polar angle φ remains the same, the polar radius r is projected onto an arc with the center angle ρ , where

$$\mathcal{C}: \tan \frac{\rho}{2} = r = ae^{b\varphi}. \tag{3.1}$$

The Logarithmic Spiral and its Spherical Counterpart

Since the stereographic projection preserves angles, the image obtained on the sphere is a curve with constant course angle ψ , i.e., a *spherical loxodrome* \mathcal{C} with both the North-pole N and the South-pole S as asymptotic points for $\varphi \rightarrow -\infty$ and $\varphi \rightarrow \infty$, respectively.

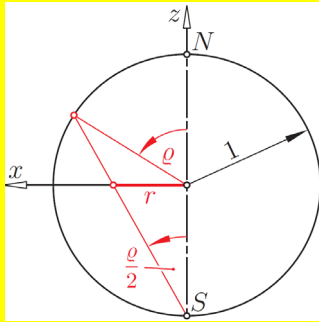


Fig. 12 Stereographic projection.

In order to parametrize the unit sphere, we use the spherical distance ρ to the North-pole N and the polar angle φ . This results in

$$\mathbf{x}(\rho, \varphi) = \begin{pmatrix} \sin \rho \cos \varphi \\ \sin \rho \sin \varphi \\ \cos \rho \end{pmatrix}. \quad (3.2)$$

The parameter lines $\varphi = \text{const.}$ are meridians, the lines $\rho = \text{const.}$ parallel circles. We obtain an orthogonal net with tangent vectors

$$\mathbf{x}_\rho = \begin{pmatrix} \cos \rho \cos \varphi \\ \cos \rho \sin \varphi \\ -\sin \rho \end{pmatrix} \text{ and } \mathbf{x}_\varphi = \begin{pmatrix} -\sin \rho \sin \varphi \\ \sin \rho \cos \varphi \\ 0 \end{pmatrix}, \quad (3.3)$$

where $\|\mathbf{x}_\rho\| = 1$, $\|\mathbf{x}_\varphi\| = \sin \rho$, and $\mathbf{x}_\rho \cdot \mathbf{x}_\varphi = 0$.

The spherical loxodrome can be represented as

$$\mathcal{C}: \mathbf{c}(\varphi) = \begin{pmatrix} \sin \rho \cos \varphi \\ \sin \rho \sin \varphi \\ \cos \rho \end{pmatrix}, \text{ where } \tan \frac{\rho}{2} = ae^{b\varphi} \quad (3.4)$$

for $-\infty < \varphi < \infty$. This confirms that $\lim_{\varphi \rightarrow \infty} \rho(\varphi) = \pi$ (South-pole) and $\lim_{\varphi \rightarrow -\infty} \rho(\varphi) = \pi$ (North-pole).

Upon differentiate of the last equation in eq. (3.4) w.r.t. φ , we obtain

$$\left(1 + \tan^2 \frac{\rho}{2}\right) \frac{d\rho}{2d\varphi} = abe^{b\varphi}, \quad \frac{d\rho}{d\varphi} = 2b \tan \frac{\rho}{2} \cos^2 \frac{\rho}{2}$$

hence, by virtue of eq. (2.3),

$$\dot{\rho} := \frac{d\rho}{d\varphi} = 2b \sin \frac{\rho}{2} \cos \frac{\rho}{2} = b \sin \rho = \cot \psi \sin \rho. \quad (3.5)$$

For the velocity vector of \mathcal{C} we obtain, in turn,

$$\dot{\mathbf{c}} := \frac{d\mathbf{c}}{d\varphi} = \dot{\rho} \mathbf{x}_\rho + \mathbf{x}_\varphi \text{ with } \|\dot{\mathbf{c}}\|^2 = (b^2 + 1) \sin^2 \rho, \quad (3.6)$$

which yields, for the arc-length s of \mathcal{C} , with an appropriate initial point and orientation,

$$ds = \|\dot{\mathbf{c}}\| d\varphi = \frac{\sin \rho}{\sin \psi} d\varphi = \frac{\dot{\rho}}{b \sin \psi} d\varphi = \frac{1}{\cos \psi} d\rho.$$

Moreover,

$$s = s(\varphi) = \frac{1}{\cos \psi} (\rho(\varphi) - \rho(0)) = \frac{1}{\cos \psi} (\rho(\varphi) - \alpha) \quad (3.7)$$

with $\alpha = \rho(0) = 2 \arctan a = \text{const.}$ and the limits $s(\infty) = (\pi - \alpha) / \cos \psi$ and $s(-\infty) = -\alpha / \cos \psi$. Hence, the total arc-length of the loxodrome between the North- and the South-pole is $\pi / \cos \psi$.

From eq. (3.7) we conclude that, similar to the planar case, the arc length parametrization of \mathcal{C} in (3.4) is given by

$$\rho(s) = \alpha + s \cos \psi > 0 \text{ and } \varphi(s) = \frac{1}{b} \left[\ln \left(\tan \frac{\rho}{2} \right) - \ln \left(\tan \frac{\alpha}{2} \right) \right]. \quad (3.8)$$

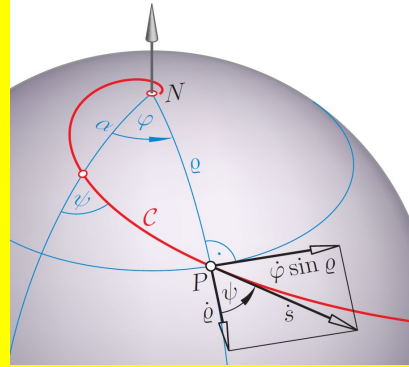


Fig. 13 The spherical distance ρ is a linear function of $s \Leftrightarrow \psi = \text{const.}$

Similar to the planar case, depicted in Fig. 1, we deduce from the decomposition of the velocity vector $\dot{\mathbf{c}}$ in (3.6) that the function $\rho(s)$ is linear if and only if the angle ψ with $\cos \psi = \dot{\rho} / \dot{s}$ is constant (see Fig. 13), where $\|\dot{\mathbf{c}}\| = \dot{s}$.

Lemma 2: *Spherical loxodromes are characterized by the spherical polar distance ρ being a linear function of arc length s .*

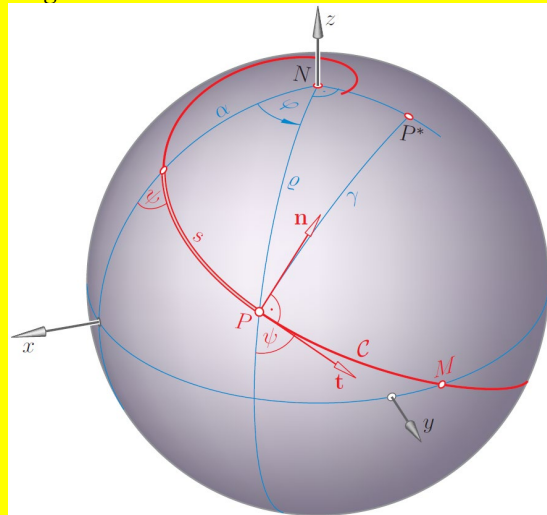


Fig. 14 Spherical loxodrome \mathcal{C} with the spherical radius of curvature γ and the center of curvature P^* at P .

The unit tangent vector \mathbf{t} and the normal vector \mathbf{n} of the loxodrome \mathcal{C} (see Fig. 14) are

$$\mathbf{t} = \frac{d\mathbf{c}}{ds} = \cos \psi \mathbf{x}_\rho + \frac{\sin \psi}{\sin \rho} \mathbf{x}_\varphi, \quad \mathbf{n} = -\sin \psi \mathbf{x}_\rho + \frac{\cos \psi}{\sin \rho} \mathbf{x}_\varphi.$$

Differentiation of \mathbf{t} w.r.t. s gives, according to the Frenet equations,

$$\frac{d\mathbf{t}}{ds} = -\mathbf{c} + \kappa_g \mathbf{n}$$

with κ_g as the geodesic curvature of \mathcal{C} . After some manipulations, we obtain

$$\kappa_g = \sin \psi \cot \rho = \cot \gamma \quad (3.9)$$

with γ being the spherical radius of curvature, as depicted in Fig. 14. Moreover, P^* is the spherical center of curvature, i.e., the spherical center of the osculating circle. A positive geodesic curvature means that the curve turns left when moving along a path with an increasing parameter s . Note that the midpoint M of \mathcal{C} with $\rho = \pi/2$ is a spherical inflection point, i.e., with $\kappa_g = 0$. When passing along \mathcal{C} , the sign of κ_g changes at this point, M , on the equator.

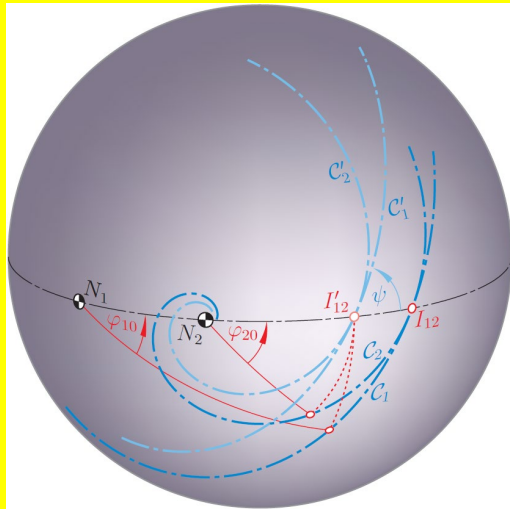


Fig. 15 Non-uniform transmission from N_1 to N_2 via rolling spherical loxodromes \mathcal{C}_1 and \mathcal{C}_2 .

The linearity of the function $\rho(s)$, by virtue of (3.8), reveals that two congruent loxodromes $\mathcal{C}_1, \mathcal{C}_2$ with fixed asymptotic points N_1, N_2 can roll on each other, internally or externally (Fig. 15). Similarly to the planar case, depicted in Fig. 6, the reason behind is that either the difference or the sum of distances ρ_1 and ρ_2 of the pitch point to the fixed centers N_1 and N_2 remains constant. When one of the two rolling loxodromes remains fixed, the asymptotic points of the other loxodrome trace circles.

As well, whereby applying the Camus theorem in the spherical case, loxodromes are the auxiliary centrodes required for generating spherical involute gears. We can verify this as given below.

When one loxodrome \mathcal{C}_2 rolls on a fixed circle \mathcal{C}_1 , as shown in Fig. 16, the asymptotic point N_2 of \mathcal{C}_2 traces an involute o of the base circle b_1 concentric with \mathcal{C}_1 . The same holds for the other asymptotic point S_2 . As in the plane, this follows from the constancy of angle ψ between the path normals and the circle \mathcal{C}_1 . However, the trajectory o of point N_2 ends outside \mathcal{C}_1 , since infinitely many rotations would be necessary until N_2 reaches the fixed circle. Therefore, a second spherical loxodrome $\bar{\mathcal{C}}_2$ is needed for tracing the complete involute. At the dis-

played position of $\bar{\mathcal{C}}_2$, the asymptotic point becomes stationary at a cusp of o . The reason behind stationarity is an instant triple-point-contact between $\bar{\mathcal{C}}_2$ and \mathcal{C}_1 .

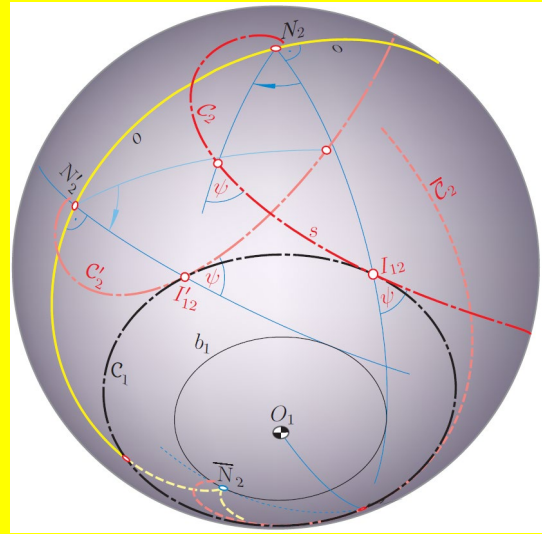


Fig. 16 While the loxodrome \mathcal{C}_2 with course angle $\psi = 53.0^\circ$ rolls on circle \mathcal{C}_1 , the asymptotic point N_2 traces a spherical involute o of the base circle b_1 .

The foregoing results are summarized below.

Theorem 3: Table 2 shows trajectories of the asymptotic points N_2 and S_2 of a spherical loxodrome \mathcal{C}_2 when rolling on specific curves.

Table 2

Rolling spherical loxodromes

spherical loxodrome \mathcal{C}_2 rolls on	paths of asymptotic points N_2, S_2	Figs.
a congruent spherical loxodrome \mathcal{C}_1	circles centered at a pole N_1 of \mathcal{C}_1	
a circle \mathcal{C}_1	involutés of a concentric circle b_1	Fig. 16

Remark 2: There is no spherical counterpart of the two-fold-decomposable two-parametric rollings of logarithmic spirals (Theorem 1) since no parallelograms exist in spherical geometry. Moreover, any spherical counterpart of the specific rolling depicted in Fig. 9 is missing since there do not exist spherical similarities other than motions.

In Fig. 17, we illustrate another role of spherical loxodromes. In the projective model of hyperbolic geometry, the sphere can be seen as a Clifford surface, i.e., as the locus of points at constant (hyperbolic) distance to an axis. Then, the loxodrome is a hyperbolic helical curve. Similarly to the Euclidean 3-space, we can use helical curves on a Clifford surface to build various grids. Figure 17 shows a 3-web, consisting of three types of regularly distributed spherical loxodromes with common asymptotic points but different course angles ψ_1, ψ_2 and ψ_3 . Each curved triangle has the same interior angles.

Another approach to this 3-web can be based on the conformal Mercator projection of the sphere into a plane, as per Marcotte and Salomone in [16]. This transfor-

mation maps loxodromes with a common course angle ψ into parallel straight lines. The 3-web, as displayed in Fig. 17, corresponds to a planar web formed by three families of parallel straight lines.

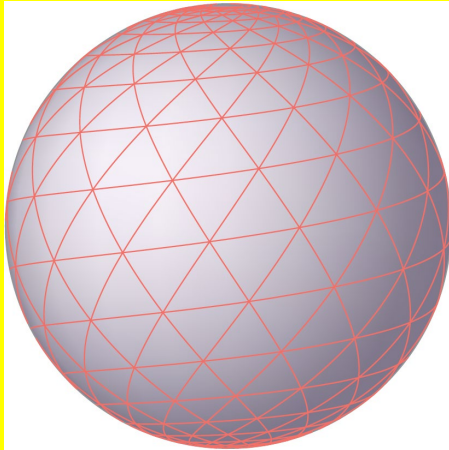


Fig. 17 3-web of spherical loxodromes.

4. CONCLUSION

The kinematic properties of planar and spherical logarithmic spirals were analyzed, with the purpose of studying specific trajectories when these spirals were rolling on lines, circles or, again, on logarithmic spirals. In particular, when the planar and the spherical logarithmic spirals are used as auxiliary centrodes, and the corresponding asymptotic points as tracing points, the planar and spherical involute tooth profiles can be generated via the Camus theorem (cf [13]). This could be useful to synthesize the spatial version of the logarithmic spiral and the skew involute gears.

REFERENCES

[1] Airy, G.B.: *On the forms of the teeth of wheels*. Transactions of the Cambridge Philosophical Society, 1825, Vol. II, Part I., pp. 277–286.

[2] Bennett, J.A.: *George Biddell Airy and horology*. Annals of Science **37**, (3), 269–285 (1980).

[3] Bool, F.H., Kist, J.R., Locher, J.L., Wierda, F.: *M.C. Escher: His Life and Complete Graphic Work*. Harry N. Abrams, Inc., New York 1992.

[4] Bricard, R.: *Sur les mouvements plans à deux paramètres doublement décomposables*. Bulletin Société de la Mathématique de France, Comptes Rendus des Séances, **41**, 27–29 (1913).

[5] Bricard, R.: *Sur une hexaédre particulier*. Nouvelles annales de mathématiques, Série 4, **13**, 24–29 (1913).

[6] Bricard, R.: *Sur les mouvements doublement décomposables*. Comptes Rendus Hebdomadaires des Séances de l'académie des sciences **158**, 110–112 (1914).

[7] Bricard, R.: *Sur un mouvement plan à deux paramètres, doublement décomposables*. Nouvelles annales de mathématiques, Série 6, **2**, 105–109 (1927).

[8] Bricard, R.: *Leçons des Cinématique, Tome 2*. Gauthier-Villars et Cie, Paris 1927.

[9] Figliolini, G., Angeles, J.: *Algorithms for involute and octoidal bevel-gear generation*. ASME J. of Mechanical Design **127**/4, 664–672 (2005).

[10] Figliolini, G., Rea, P., Angeles, J.: *Synthesis of the pitch surface of non-circular skew-gears*. Proc. of the ASME 2010 IDETC-CIE Conference, Aug. 2010, Montreal/Quebec, Canada, Paper: DETC2010-28902.

[11] Figliolini, G., Stachel, H., Angeles, J., *A new look at the Ball-Disteli diagram and its relevance to spatial gearing*. Mechanism and Machine Theory **42**/10, 1362–1375 (2007).

[12] Figliolini, G., Stachel, H., Angeles, J.: *The role of the orthogonal helicoid in the generation of the tooth flanks of involute-gear pairs with skew axes*. ASME J. of Mechanisms and Robotics **7**/1, 011003, 9 pages, (2015).

[13] Figliolini, G., Stachel, H., Angeles, J., *Kinematic Properties of Planar and Spherical Logarithmic Spirals: Applications to the Synthesis of Involute Tooth Profiles*. Mechanism and Machine Theory, <https://doi.org/10.1016/j.mechmachtheory.2019.02.010>

[14] Koenigs, G.: *Sur les mouvements doublement décomposables et sur les surfaces qui sont le lieu de deux familles des courbes égales*. Comptes Rendus Hebdomadaires des Séances de l'académie des sciences **157**, 988–991 (1913).

[15] Krysz, V., Mostyn, V., Kot, T.: *The synthesis and testing of a shaped wheel for stairs climbing robot*. Appl. Mech. Mater. **555**, 178–185 (2014).

[16] Marcotte, J., Salomone, M.: *Loxodromic Spirals in M.C. Escher's Sphere Surface*. J. Humanist. Math. **4**/2, 25–46 (2014).

[17] Mostyn, V., Krysz, V., Kot, T., Bobovsky, Z., Novak, P.: *The synthesis of a segmented stair-climbing wheel*. Int. J. Adv. Robot. Syst. **15**/1, 1–11 (2018).

[18] Reuleaux, F., *The Kinematics of Machinery*, Dover Publications Inc., New York 1963, pp. 155–156.

[19] Stachel, H.: *A Family of Multiply Decomposable Euclidean Motions*. In I. Bárány, K. Böröczky (eds.): *Intuitive Geometry*. Bolyai Society Mathematical Studies 6, János Bolyai Mathematical Society, Budapest 1997, pp. 413–427.

[20] R. Willis: *Principles of mechanism*. 2nd ed., Longmans, Green and Co., London 1870.

[21] W. Wunderlich: *Ebene Kinematik*. Bibliographisches Institut, Mannheim, Wien, Zürich 1970.

Authors:

Prof. Hellmuth STACHEL, Professor emeritus, Institute of Discrete Mathematics and Geometry, Vienna University of Technology, Vienna, Austria, E-mail: stachel@dmg.tuwien.ac.at, tel: +431 58801 10434

Prof. Giorgio FIGLIOLINI, Dept. of Civil and Mechanical Engineering, University of Cassino and Southern Lazio, Cassino, Italy, E-mail: figliolini@unicas.it.

Prof. Jorge ANGELES, Department of Mechanical Engineering & CIM, McGill University, Montreal, Canada, E-mail: angeles@cim.mcgill.ca.